Environmental Science Nano

Nanoparticle Aggregation in a Freshwater River: The Role of Engineered Surface Coatings

Journal:	*Environmental Science: Nano*
Manuscript ID	EN-ART-09-2018-001021.R2
Article Type:	Paper
Date Submitted by the Author:	14-Dec-2018
Complete List of Authors:	Surette, Mark; Oregon State University, Chemical, Biological, and Environmental Engineering Nason, Jeffrey; Oregon State University, Chemical, Biological and Environmental Engineering

Nanoparticle Aggregation in a Freshwater River: The Role of Engineered Surface Coatings

*Mark C. Surette and Jeffrey A. Nason**

School of Chemical, Biological and Environmental Engineering

Oregon State University, 116 Johnson Hall, 105 SW 26th St., Corvallis, OR 97331

ENVIRONMENTAL SIGNIFICANCE STATEMENT

An important process affecting the environmental fate of engineered nanoparticles (ENPs) is aggregation. It is well-established that in model aquatic mediums this process can be affected by engineered surface coatings applied to ENPs. Yet, their role in affecting ENP aggregation within complex aquatic mediums is poorly understood. We find that ENP colloidal stability is linked to eco-corona formation (i.e., adsorption of natural organic matter). Neutral or negatively-charged, covalently-bound surface coatings prevented homo- and heteroaggregation in river water while positively-charged or electrostatically-bound surface coatings allowed aggregation to occur. Under the conditions tested, homoaggregation was the dominant mode of aggregation, despite the presence of natural colloids. This work advances our understanding of how surface coatings can influence the environmental fate of ENPs.

ABSTRACT

Within aquatic environments, the aggregation of ENPs has been identified as an important process affecting their environmental fate. Previous research using simple model mediums has demonstrated that engineered surface coatings applied to ENPs can alter their aggregation behavior. However, the relevance and effect of these surface coatings on ENPs dispersed in complex aquatic mediums is largely unknown. The objective of the current work was to explore this topic further using gold nanoparticles (AuNPs) with different engineered surface coatings as model ENPs. AuNPs with neutral or negatively-charged, covalently-bound surface coatings (polyethylene glycol [PEG] or carboxylated PEG, respectively) were found to be stable in both raw and filtered river water, while AuNPs with positively-charged (branched polyethylenimine, aminated PEG) or electrostatically-bound (citrate) surface coatings readily aggregated. For the model ENPs that aggregated, their average percent removal after mixing in the filtered river water was similar to that measured after the same period in raw river water, revealing that homoaggregation was dominant relative to heteroaggregation. To quantify the effect of the surface coatings on the colloidal stability of the model ENPs, we attempted to estimate homo- and heteroaggregation attachment efficiency factors (α_{homo} and α_{hetero}, respectively) using a recently reported functional assay. A number of challenges preventing these direct calculations in this system are discussed. However, from modelling it was inferred that $\alpha_{homo} \geq \alpha_{hetero}$. We find that ENP colloidal stability was related to eco-corona formation (i.e., adsorption of natural organic matter), which was regulated by the properties of the engineered surface coatings. Overall, the results of the batch experiments demonstrate that engineered surface coatings can affect ENP colloidal stability in a complex medium, further highlighting the need to consider this factor when investigating the environmental fate of ENPs.

INTRODUCTION

Currently, there is a lack of data regarding the concentration of engineered nanoparticles (ENPs) in the environment. Researchers and regulators examining the implications of ENPs currently rely on environmental fate and transport models to define environmentally-relevant exposure concentrations. This reliance is partly due to challenges with the detection and analysis of ENPs in the environment.[1,2] Substantial work has been done to adapt multimedia environmental fate models originally developed for organic chemicals to capture the processes relevant to ENPs.[3–5] Among other insights, these models have shown that within aquatic environments the aggregation of ENPs is an important physical-chemical process affecting their environmental fate. While there remains some debate regarding the appropriate fate descriptors to use when modelling particle aggregation[6–8], current environmental fate models have adopted the use of particle-based rate constants to describe this process (e.g., $k_{hetero} = \alpha_{hetero} \times k_{coll.}$). To refine their predictive capability, the parameters used in modelling particle aggregation require accurate quantification under environmentally relevant conditions.[9–12]

When particles aggregate, there are two types of particle interactions to consider—those between similar particles (homoaggregation) and those between dissimilar particles (heteroaggregation). An important parameter used in modelling either type of particle interaction is the attachment efficiency factor (α_{homo} or α_{hetero}, respectively). These factors account for short-range forces that are not well-defined mechanistically but nonetheless effect the likelihood that particle collisions will result in attachment. When assessing particle aggregation, simplified model aquatic mediums are typically used.[13,14] This approach enables systematic investigations of individual factors influencing ENP aggregation, such as natural macromolecules (e.g., proteins, humic and fulvic acids, etc.)[15,16] and the chemistry of the surrounding aquatic medium.[17,18] It also permits the effect of those factors to be quantified using established methods to estimate α_{homo} and α_{hetero}.[19–21] A limitation of this approach, however, is that it does not capture the inherent complexity of real environmental mediums.[22]

Previous research using model aquatic mediums has shown that an important factor affecting the colloidal stability of ENPs is their surface coating.[23] These surface coatings can be intentionally applied to ENPs during their production (herein termed 'engineered surface coating') or acquired via interactions between the ENP and naturally occurring macromolecules (often termed 'eco-corona'). Regardless of their origin, surface coatings can influence ENP environmental fate. For example, the presence of different engineered surface coatings on gold nanoparticles dispersed in model aquatic mediums have been shown to alter the adsorption of natural macromolecules to ENPs and effect their colloidal stability.[24,25] From the perspective of modelling ENP aggregation in real environmental systems, however, it is unknown if the results obtained in the model aquatic mediums are still applicable. Thus arises a significant challenge—how best to translate the results of mechanistic investigations into predictions of ENP fate in complex environmental mediums. While engineered surface coatings have been shown to be a relevant factor influencing ENP stability in model aquatic mediums, whether they remain relevant in a real environmental medium has yet to be determined. It is hypothesized that in a real aquatic medium an ENP's engineered surface coating will influence eco-corona formation and in turn affect the aggregation behavior of the ENPs.

The main objective of this work was to examine whether the aggregation behavior of ENPs dispersed in a real aquatic medium was affected by their engineered surface coating. To accomplish this, the colloidal stability of gold nanoparticles (AuNPs) stabilized with five different engineered surface coatings was assessed in raw and filtered river water using a protocol adapted from Barton et al. (2014). Samples of the river water were spiked to an ENP mass concentration of 500 µg/L, lower than is typically used when investigating particle aggregation.[19–21] The raw river water contained naturally-occurring colloids at their native concentration to accurately represent environmentally relevant conditions. The results were compared with previous research using model aquatic mediums to help bridge the gap between

these different approaches and assess whether engineered surface coatings are a relevant factor affecting the aggregation of ENPs in a complex aquatic medium.

In addition to reporting on the effects of engineered surface coatings on ENP aggregation, we attempted to quantify their effect via estimating α_{homo} and α_{hetero}. To accomplish this, the functional assay detailed by Wiesner and colleagues regarding the 'surface affinity' parameter was evaluated. This assay has been used to evaluate the heteroaggregation of ENPs in activated sludge, probe the uptake and trophic transfer of model ENPs in a simplified food web, and investigate the attachment of silver nanoparticles with various surface coatings to different model collectors (glass beads and kaolinite).[26–30] These studies demonstrate the utility of this assay for comparing the relative aggregation behavior of ENPs in different matrices and correlating that behavior with important environmental outcomes like uptake and transport. For the current work we discuss the challenges and limitations of working in the experimental space required by this functional assay.

MATERIALS AND METHODS

Engineered Nanoparticles

Gold nanoparticles (AuNPs) with core diameters of 10.5 – 15 nm were selected as model ENPs. Each AuNP was stabilized by one of five different engineered surface coatings: 2 kiloDalton (kDa) polyethylenegylcol (PEG), 3 kDa carboxyl-functionalized PEG (PEG-COOH), 3 kDa amine-functionalized PEG (PEG-Amine), 25 kDa branched polyethylenimine (bPEI), and citrate (Cit). Manufacturer reported specifications and measured characteristics for the model ENPs are provided in Table 1. The PEG-, bPEI-, and Cit-AuNPs were purchased from nanoComposix, Inc. (NanoXact 0.05 mg/mL) while the PEG-COOH- and PEG-Amine-AuNPs were purchased from Cytodiagnostics (carboxyl-PEG3000-SH and amine-PEG3000-SH, respectively). As detailed in the

Supplementary Information (Table S1), the difference in the intensity-weighted hydrodynamic diameter (D_h) and core diameter (D_c) reported in Table 1 is attributed to the presence of few, small aggregates and/or particle contaminants in the samples during measurement. Per the number-weighted D_h, the majority of the model ENPs had primary particle sizes of ≈20 – 30 nm (Table S1), which is within expectations given the engineered surface coatings possessed by the model ENPs.

Table 1. Manufacturer reported specifications and measured characteristics of model ENPs.

Surface Coating	Core-Surface Coating Binding Mechanism	Core Diameter (nm)[a]	*Z*-Average Hydrodynamic Diameter (nm)[b]	Zeta Potential (mV)[c]
2 kDa PEG	Covalent (Thiol)	10.5	34.4 ± 7.4	-25.9 ± 4.2 (pH 6.8 ± 0.03)
3 kDa PEG-COOH	Covalent (Thiol)	15	52.5 ± 12.4	-25.9 ± 4.2 (pH 7.1 ± 0.1)
3 kDa PEG-Amine	Covalent (Thiol)	15	59.0 ± 15.3	-14.9 ± 2.1 (pH 7.0 ± 0.1)
25 kDa bPEI	Covalent (Thiol)	12.1	40.4 ± 8.9	+25.4± 2.1 (pH 6.8 ± 0.1)
Citrate	Electrostatic	15	61.7 ± 39.8	-47.5 ± 4.2 (pH 7.4 ± 0.1)

Error bars indicate ± 95% confidence interval.

[a] Per manufacturer's specifications, measured via transmission electron microscopy (TEM).

[b] Measured via dynamic light scattering (DLS) at 1-10 mg Au/L in 0.02 µm filtered 18.2 MΩ-cm distilled, deionized water (DDI; EGLA Purelab); (PEG) n = 4; (PEG-COOH) n = 7; (PEG-Amine) n = 7; (bPEI) n = 2; (Cit) n = 4.

[c] Measured in pH-adjusted 1 mM KCl at 10 mg Au/L at the pH listed in parentheses; n = 15. Calculation of the zeta potential (ζ) from measured electrophoretic mobility (EPM) is detailed in Supplementary Information.

Complex Aquatic Medium

The Willamette River (Oregon, USA) receives effluent from multiple sources that may release ENPs to the environment (e.g., storm water, agricultural runoff, industrial and municipal wastewater), making it a representative medium to study the environmental fate and transport of ENPs. Samples of Willamette River water (WRW) were collected from the intake line to the City of Corvallis' municipal drinking water treatment facility (H.D. Taylor Water Treatment Plant, Corvallis, OR). In total, approximately 15 L of WRW were collected on June 30, 2017 using acid-washed 1-L high-density polyethylene (HDPE) containers (Nalgene®). Prior to sample collection, the containers were rinsed with river water and then filled to minimize the headspace in the container. Water quality characteristics of the WRW were measured within 21-days of sample

collection per method-specific holding times. A portion of WRW was sequentially filtered through 0.45 µm (Supor®, Pall Corporation) and 0.02 µm (Anotop®, Whatman) filters following the procedures outlined by Karanfil et al. (2003) to limit organics leaching from the filters. A summary of the measured water quality characteristics is provided in Table 2. Additional details regarding the preparation and analysis of the WRW are provided in the Supplementary Information (Tables S4 and S5).

Table 2. Water quality characteristics of the Willamette River water sampled on June 30, 2017.

Parameter	Value	
Dissolved Organic Carbon (DOC)	0.83 ± 0.1	mg C/L
Ionic Strength	0.68	mM
pH	7.9 ± 0.1	
Total Suspended Solids (TSS)	3.9 ± 0.4	mg/L
Total Alkalinity	25.0	mg/L as $CaCO_3$
Total Hardness	18.6	mg/L as $CaCO_3$

Error bars indicate ± one standard deviation of the mean (n = 3).

Batch Experiments

Six separate 50-mL batches were prepared for each AuNP type: three containing 0.02 µm filtered WRW to examine the effects of homoaggregation in isolation and three containing raw WRW to examine the combined effects when both homo- and heteroaggregation are possible. All batch experiments were completed within ten days of collecting the WRW. Each batch was continuously-stirred at 400 rpm, corresponding to an average shear rate of 15.6 s^{-1} (Table S6).[32] Upon mixing, each batch was dosed to an AuNP mass concentration ($C_{NP,0}$) of 500 µg Au/L,

equivalent to an initial number concentration ($N_{NP,0}$) of 1.5 – 4.3 $x10^{13}$ particles/L depending on the Au core diameter. This mass concentration, while higher than the expected mass concentration of ENPs in the environment (e.g., ng/L – μg/L), was chosen to balance representativeness while minimizing analytical complications that arise at lower concentrations.[9] Upon dosing, the temperature (T = 25 ± 1 °C) and pH (pH 7.9 ± 0.1) of each batch were recorded.

Each batch was continuously mixed for 480 minutes, with 5-mL aliquots collected from each batch at predetermined time-points. Upon collection, each aliquot was immediately centrifuged at 3,500 rpm (≈2,200*g* RCF) for 2 minutes. This centrifugation speed and duration was found to remove large natural colloids (d_{NC} ≥ ≈300 nm) and ENP-containing aggregates while minimizing the removal of unaggregated ENPs (Tables S7 – S10). However, it is possible that very small ENP-containing aggregates may have remained in suspension following the centrifugation step (see Supplementary Information for details). After centrifugation, the supernatant (V = 4 mL) was removed, transferred to a perfluoroalkoxy alkane (PFA) vial, and acid-preserved via the addition of 10 μL of concentrated (70% w/w), ultra-pure HNO_3 (VWR International). Once all the aliquots were collected, they were acid-digested using freshly prepared *aqua regia* (3:1 ultra-pure HCl:HNO_3; see Supplementary Information for details) and then analyzed via inductively-coupled plasma optical emission spectroscopy (ICP-OES; Spectro Analytical Instruments) to quantify the AuNP number concentration in the supernatant ($N_{NP,i}$) at each time-point.

Time-Resolved Dynamic Light Scattering

To substantiate the trends observed in the batch experiments, time-resolved dynamic light scattering (TR-DLS) measurements were performed. Since DLS is not capable of distinguishing between model ENPs and background natural colloids (NCs), the technique was limited to the filtered WRW. Briefly, 3.5 mL samples containing the filtered WRW were dosed with a given

model ENP to C_{NP} = 500 µg Au/L, matching the conditions of the batch experiments. Upon dosing, the intensity-weighted hydrodynamic diameter (D_h) was measured over time (120 measurements, each 15 seconds long) using a Brookhaven 90-Plus particle size analyzer (Brookhaven Instrument Corporation). Using the TR-DLS data, the colloidal stability of the model ENPs was assessed by calculating the extent of aggregation ($D_{h,final}/D_{h,initial}$) and the initial aggregation rates ($dD_h/dt|_{t\to 0}$) according to the procedures described previously.[25,33]

Electrophoretic Mobility

Electrophoretic mobility (EPM) measurements were conducted to investigate the surface charge of the model ENPs in WRW. Due to the same limitations as the DLS, the EPM analytical technique was limited to the filtered WRW. To probe the effect of the natural organic matter (NOM) in the WRW on the surface charge of the model ENPs, measurements were also conducted using a synthetic water that mimicked the pH, ionic strength, and the ionic composition of the WRW but did not contain any NOM (Table S12). For each sample, 1.5 mL of the chosen medium was spiked with a given model ENP to C_{NP} = 500 µg Au/L, matching the conditions of the batch and TR-DLS experiments. The samples were allowed to incubate for 30 minutes before the EPM of the sample was measured (5 measurements of 30 cycles each) using a Brookhaven ZetaPALS (Brookhaven Instrument Corporation).[25]

RESULTS AND DISCUSSION

Filtered River Water

The loss of ENPs from homoaggregation was assessed by calculating the average percent removal (η) in filtered WRW after 480 minutes (Figure 1a). The PEG-AuNPs were highly resistant to aggregation, with negligible removal at the completion of the batch experiment. Likewise,

only minimal removal of the PEG-COOH-AuNPs was observed (η = 18 ± 10%; mean ± 95% confidence interval [n = 3]). The remaining three model ENPs were removed to varying degrees: the Cit-AuNPs to a moderate extent (η = 37 ± 23%) and the bPEI- and PEG-Amine-AuNPs more significantly (η = 75 ± 15% and 78 ± 5%, respectively).

Time-resolved dynamic light scattering (TR-DLS) was used to confirm these trends and calculate the extent of aggregation ($D_{h,final}/D_{h,initial}$) and the initial aggregation rates ($dD_h/dt|_{t\to 0}$). Values of $D_{h,final}/D_{h,initial} \approx 1$ denote particle stability whereas $D_{h,final}/D_{h,initial} > 1$ indicates that particles are aggregating. The TR-DLS measurements show that the PEG- and PEG-COOH-AuNPs were stable while the PEG-Amine- and bPEI-AuNPs readily homoaggregated (Figure 1b). The Cit-AuNPs underwent homoaggregation during the TR-DLS measurement period, however, $D_{h,final}/D_{h,initial}$ was much lower compared to the PEG-Amine- and bPEI-AuNPs. This is consistent with the initial aggregation rate, which indicates that the Cit-AuNPs aggregated more slowly compared to the PEG-Amine- and bPEI-AuNPs (Figure 1b).

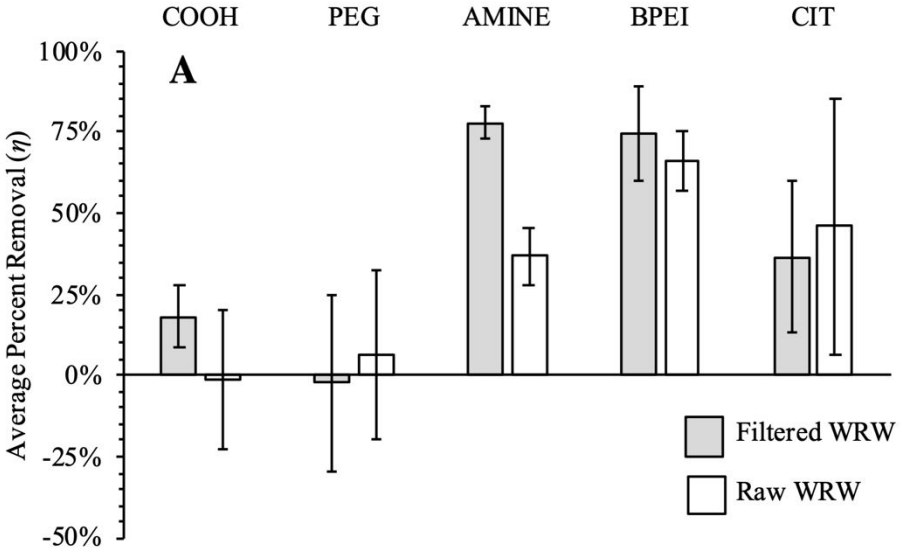

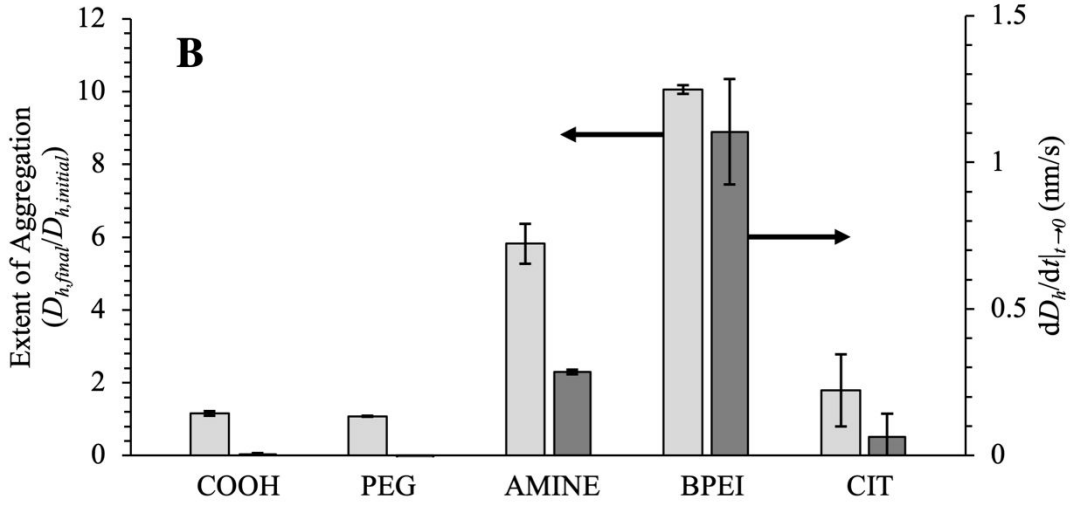

Figure 1. (a) Average percent removal (η) for each model ENP after 480 minutes. Error bars indicate ± 95% confidence interval (n = 3). **(b; left)** Average extent of aggregation ($D_{h,final}/D_{h,initial}$) after 30 minutes **and (b; right)** initial aggregation rate ($dD_h/dt|_{t\to 0}$) for each model ENP in filtered WRW. Error bars indicate ± one standard deviation (n = 2 – 3).

Overall, the results from the TR-DLS measurements match the observations from the batch experiments. In combination they reveal that the Cit-, bPEI-, and PEG-Amine-AuNPs were destabilized in the filtered WRW and underwent homoaggregation. Furthermore, the extent of aggregation measured via TR-DLS tracks the removal measured in the batch experiments. The PEG-Amine- and bPEI-AuNPs, which rapidly homoaggregated, were removed to a greater degree during the batch experiments while the Cit-AuNPs, which homoaggregated more slowly, were removed to a lesser extent. The TR-DLS data for each model ENP is provided in the Supplementary Information (Table S13 and Figure S4).

The EPM measurements for all five model ENPs in synthetic and filtered WRW are shown in Figure 2. In both mediums the PEG- and PEG-COOH-AuNPs had slightly negative EPM that did not vary with the suspending medium (PEG: paired *t*-test(14) = 0.37, $p = 0.72$; PEG-COOH: paired *t*-test(14) = 0.35, $p = 0.73$). In contrast, the EPM of the PEG-Amine-, bPEI-, and Cit-AuNPs did vary when suspended in the two mediums. The PEG-Amine- and bPEI-AuNPs had positive EPM in the synthetic WRW whereas they had negative EPM in the filtered WRW (bPEI: paired *t*-test(9) = 5.93, $p \ll 0.01$; PEG-Amine: paired *t*-test(14) = 15.62, $p \ll 0.01$). The Cit-AuNPs had negative EPM in both the synthetic and filtered WRW; however, their EPM was more negative in the filtered WRW (paired *t*-test(14) = 2.99, $p = 0.01$). For all five model ENPs the EPM measured in the synthetic WRW differed from the baseline measurements conducted in pH-adjusted 1 mM KCl (Table 1). The cause for this is unclear, as the ionic strength of the synthetic WRW is slightly lower ($I = 0.68$ mM) than the simple electrolyte medium and the pH is similar. This disparity may be attributable to the presence of polyvalent ions in the synthetic WRW.

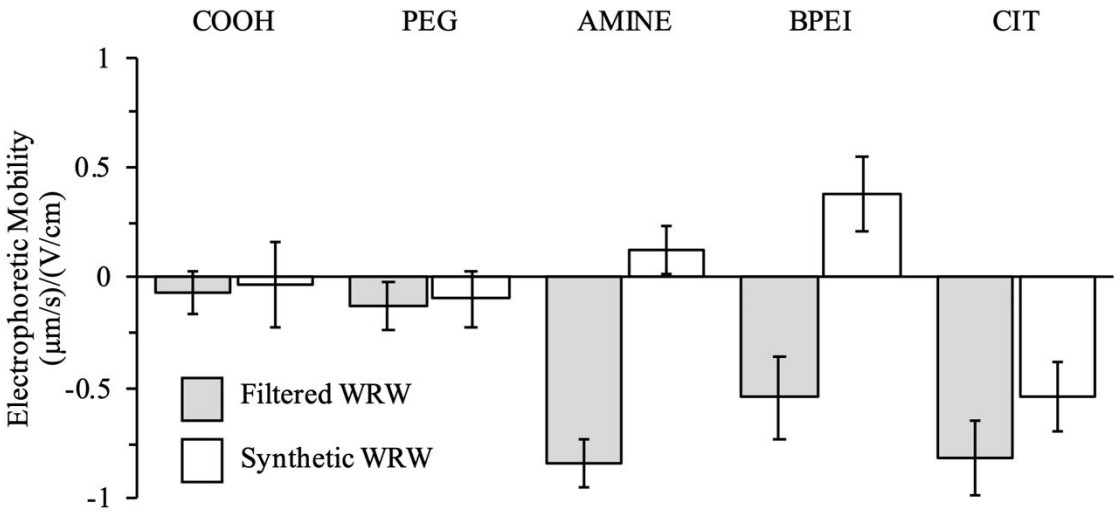

Figure 2. Electrophoretic mobility (EPM) of each model ENP in filtered WRW at pH 7.6 ± 0.04 (hashed) and synthetic WRW at pH 7.0 ± 0.1 (solid). Error bars indicate ± 95% confidence interval (n = 10 – 15).

Comparing the findings from the current work with previous research using the same ENPs in model aquatic mediums[20,24,25] is useful to help elucidate the mechanisms affecting their colloidal stability in the filtered WRW. The PEG and PEG-COOH surface coatings were previously shown to stabilize against homoaggregation in both mono- and divalent electrolyte solutions up to I = 1.5 M and across Suwannee River NOM-to-ENP mass concentration ratios ([NOM]:[ENPs]) spanning 0 – 1.7 mg C/mg Au.[25] Thus, these surface coatings have been shown to prevent homoaggregation via electrical double-layer (EDL) compression and were not influenced by the presence of NOM at the conditions tested. The current research was performed at significantly lower ionic strength (I = 0.68 mM) that is composed of a mixture of mono- and divalent ions and at [NOM]:[ENPs] = 1.66 mg C/mg Au (see Supplementary Information Table S4). The batch experiments and TR-DLS measurements reported here show that the PEG- and PEG-COOH-AuNPs were stable at the conditions present in the filtered WRW. Individually, these model ENPs had comparable EPM in both the synthetic and filtered WRW, suggesting that these surface coatings did not adsorb NOM present in the filtered WRW. The near-neutral EPM of

these model ENPs in the filtered WRW (Figure 2) suggests that their stability may be primarily attributed to steric interactions. As a whole, the results reported herein match the trends observed using the model aquatic medium.

Like the PEG and PEG-COOH surface coatings, the PEG-Amine and bPEI surface coatings were previously found to stabilize the model ENPs against homoaggregation by EDL compression in both mono- and divalent electrolyte solutions up to I = 1.5 M.[25] However, at certain [NOM]:[ENPs] these cationic surface coatings were shown to promote homoaggregation by interparticle bridging after NOM adsorbs to the ENP surface. The EPM results in the filtered WRW demonstrate that the PEG-Amine- and bPEI-AuNPs underwent charge reversal, an indication that these surface coatings adsorbed NOM (Figure 2). Furthermore, the current work was conducted at [NOM]:[ENPs] = 1.66 mg C/mg Au, which is comparable to previous research conducted at [NOM]:[ENPs] = 1.7 mg C/mg Au.[25] In both mediums at this [NOM]:[ENPs], the PEG-Amine- and bPEI-AuNPs undergo homoaggregation. In combination, these findings would seem to suggest that NOM-facilitated interparticle bridging destabilizes the PEG-Amine- and bPEI-AuNPs in the filtered WRW. However, $D_{h,final}/D_{h,initial}$ measured in the previous work was much lower compared to that reported here (PEG-Amine: 2.50 *vs*. 5.82; bPEI: 1.96 *vs.* 10.05, respectively). This disparity may reflect the presence of polyvalent cations in the filtered WRW, which were absent from the model aquatic mediums (i.e., testing at the various [NOM]:[ENPs] was performed in 1mM KCl). This suggests that following NOM adsorption, divalent cation bridging (DCB) may be occurring in the filtered WRW. The increased $D_{h,final}/D_{h,initial}$ could also be due to variations in the NOM composition in the filtered WRW compared to the model NOM from the Suwannee River (SRNOM), as prior research has demonstrated that differences in NOM composition, in particular the molecular weight distribution, can affect colloidal stability.[16,34] However, additional testing is warranted to test this hypothesis. Overall, the aggregation behavior of the PEG-Amine- and bPEI-AuNPs is consistent with that observed in the model aquatic mediums, revealing that the mechanisms identified previously are still relevant in the filtered WRW. Namely, these model ENPs were destabilized in the filtered WRW following NOM

adsorption, either directly from NOM-facilitated interparticle bridging alone or in combination with DCB.

Finally, the electrostatically-stabilized Cit-AuNPs have been shown to readily homoaggregate following EDL compression and from DCB when in the presence of both divalent cations and NOM.[20,21,24,35] However, in the current work it is unlikely that the relatively low ionic strength (*I* = 0.68 mM) of the filtered WRW resulted in homoaggregation via EDL compression. This is based on previous research that found the Cit-AuNPs were resistant to aggregation via EDL compression in mono- and divalent electrolyte solutions at the ionic strength encountered in the current research.[21] Instead, their homoaggregation in the filtered WRW is likely due to DCB following NOM adsorption. While the Cit-AuNPs possess a negative surface charge in the filtered WRW (Figure 2), the citrate surface coating is weakly-bound to the AuNPs through electrostatic attraction. As such, NOM macromolecules possessing moieties with a stronger binding affinity (e.g., organothiols) could displace it.[36] The similarity in the EPM of the Cit-AuNPs in the filtered WRW to the NOM-coated PEG-Amine- and bPEI-AuNPs indicates that the citrate surface coating was likely displaced. This phenomena has also been observed across a wide pH range where the EPM of Cit-AuNPs was consistently lower when Suwannee River Humic Acid (SRHA) was present in the solution.[24] Following displacement of the citrate surface coating, the NOM macromolecules could then destabilize the Cit-AuNPs through either interparticle bridging alone or in combination with DCB. As with the PEG-Amine- and bPEI-AuNPs, either mechanism could be occurring; however, the results of previous work suggest that DCB may be more relevant for the citrate particles.[24]

The results from the corroborative techniques conducted with the filtered WRW demonstrate that engineered surface coatings play an influential role in determining the aggregation behavior of ENPs in a complex medium. Differences in colloidal stability were related to the way that the engineered surface coatings regulate eco-corona formation (i.e., NOM adsorption). The

negatively-charged PEG- and PEG-COOH-AuNPs did not adsorb NOM and were electrosterically stable. In contrast, the positively-charged PEG-Amine- and bPEI-AuNPs readily adsorbed NOM, undergoing charge reversal and subsequently homoaggregating. The Cit-AuNPs, which possess an electrostatically-bound, negatively-charged citrate surface coating, also homoaggregated. While the exact mechanism causing these three model ENPs to homoaggregate is unclear, the results indicate that it occurred following NOM adsorption. As such, their homoaggregation is attributed to either NOM-facilitated interparticle bridging or DCB. In the case of the citrate coating, these mechanisms likely occurred after the citrate surface coating was displaced by NOM macromolecules possessing a stronger binding affinity for the AuNP core.

Raw River Water

The experiments using the filtered WRW highlight the relevance of the engineered surface coatings in affecting the homoaggregation of the model ENPs. It is also important to assess how they influence ENP colloidal stability when natural colloids are present in the aquatic medium and heteroaggregation is possible. The loss of ENPs by aggregation in the raw WRW, the combined result of homo- and heteroaggregation, was assessed by calculating the average percent removal (η) after 480 minutes. The results, presented in Figure 1a, show that the PEG- and PEG-COOH-AuNPs underwent minimal removal (η = -6 ± 26% and 1 ± 26%, respectively). In contrast, the remaining three model ENPs were removed to varying extents: the PEG-Amine- and Cit-AuNPs to a moderate extent (η = 37 ± 9% and 46 ± 40%) and the bPEI-AuNPs to a more significant amount (η = 66 ± 9%).

The aggregation behavior of the PEG- and PEG-COOH-AuNPs was similar in the filtered and raw WRW. Thus, the electrosteric stability provided by their surface coatings not only prevents their homoaggregation, as was demonstrated in the filtered WRW, but also their heteroaggregation with the natural colloids in the raw WRW. This is attributed to the moderate molecular weight

and neutral- (PEG) or negatively-charged (PEG-COOH) surface coatings repelling the negatively-charged natural colloids (NCs).[37] The overall trends observed for the PEG-Amine-, bPEI-, and Cit-AuNPs are similar in the filtered and raw WRW. Individually the bPEI- and Cit-AuNPs were removed to comparable extents in both the filtered and raw WRW while the PEG-Amine-AuNPs were removed to a lesser extent in the raw WRW compared to the filtered WRW (paired *t*-test(2) = 13.07, $p \ll 0.01$). As the aquatic chemistry of the filtered and raw WRW are the same, it is likely that the mechanisms causing the PEG-Amine-, bPEI-, and Cit-AuNPs to homoaggregate in the filtered WRW are still affecting their colloidal stability in the raw WRW. It is also plausible that these model ENPs heteroaggregated with the NCs present in the raw WRW. As noted previously, it is possible that very small ENP-NC heteroaggregates (if formed) may have remained in suspension after centrifugation. This may account for the decrease in η for the PEG-Amine-AuNPs in the raw WRW relative to that measured in the filtered WRW. This process is also expected to be relevant for the bPEI- and Cit-AuNPs, although there was no measurable difference in η for these model ENPs between the filtered and raw WRW. Regardless, it is not possible to distinguish between homo- and heteroaggregation with our experimental approach when they are occurring simultaneously. Instead, the results obtained with the raw WRW can be compared to those obtained using the filtered WRW to provide insights into the relative importance of each process.

It was originally anticipated that removal in the raw WRW would be higher than the filtered WRW due to the additional particle-particle interactions occurring between the ENPs and the NCs in the raw WRW. The finding that removal via homoaggregation alone (filtered WRW) was comparable to or higher than the combined effect of homo- and heteroaggregation (raw WRW) conflicts with the expectation that heteroaggregation is the dominant mode of aggregation under environmentally relevant conditions.[19,38] This expectation is rooted in the assumption that the number concentration of NCs (N_{NC}) is much higher than the number concentration of ENPs (N_{NP}), thus favoring removal via heteroaggregation. To understand why our findings contradict this expectation, it is useful to assess the components driving particle aggregation and thus the

removal of the model ENPs. These components include the rate at which particle-particle interactions occur and the likelihood that particle interactions will result in attachment and the formation of particle aggregates.

The overall rate of particle-particle interactions is dependent on two, inter-related factors—the number concentration of particles in the system (i.e., N_{NP} and N_{NC}) and the frequency of particle collisions. While higher than expected in the environment, N_{NP} in the current work (1.5 – 4.3 $x10^{13}$ particles/L) was an order of magnitude or more lower than is often used when studying ENP aggregation.[19–21] Due to various challenges associated with detecting and analyzing NCs of varying composition and size, accurate estimates of N_{NC} in the raw WRW are unavailable. Particle size distribution measurements performed via Coulter Counter (Figure S1) indicate that the median d_{NC} < 0.746 µm, the instrument detection limit. This expectation is supported by previous research reporting a large fraction of N_{NC} in the range of $d_{NC} \leq 10^3$ nm, with the majority (>90%) smaller than 200 nm.[39–41] As such, values of N_{NC} were instead calculated across the range $d_{NC} = 1 – 10^4$ nm using the measured TSS (Table 2) and assuming the particles were spherical, had uniform density equal to 2.65 g/cm^3, and were represented by a single size-class (i.e., a single value of d_{NC}).

Using the known properties of the model ENPs and assumed properties of the NCs, the frequency of particle collisions was estimated (see Supplementary Information for details). For collisions involving either two model ENPs or a model ENP with a NC smaller than 5 µm, Brownian motion ($^{BR}\beta$) was the dominant collision mechanism (Figure S5). This finding was expected due to the small size of the model ENPs.[42] Up to $d_{NC} \leq 10^3$ nm, the collision frequency of two model ENPs via Brownian motion ($^{BR}\beta_{NP\text{-}NP}$) was within approximately one order of magnitude of that calculated for the collision of a model ENP and a NC via the same mechanism ($^{BR}\beta_{NP\text{-}NC}$), with the values converging as d_{NC} approaches d_{NP}.

Adjusting the estimated values of ${}^{BR}\beta_{NP\text{-}NP}$ and ${}^{BR}\beta_{NP\text{-}NC}$ to account for the short-range forces arising as two particles approach one another (i.e., ${}^{BR}[\alpha\beta]_{NP\text{-}NP}$ and ${}^{BR}[\alpha\beta]_{NP\text{-}NC}$, respectively),[42] the overall rate of particle-particle interactions via Brownian motion can be determined. In combination with N_{NP} and N_{NC} (with the latter varying with d_{NC}), the initial rate of homo- and heteroaggregation can be estimated according to Equations 1 and 2, respectively.

$$\left(\frac{dN_{NP}}{dt}\Big|_{t\to 0}\right)_{homo} = -\alpha_{homo}{}^{BR}(\alpha\beta)_{NP-NP}N_{NP}^2 \quad (1)$$

$$\left(\frac{dN_{NP}}{dt}\Big|_{t\to 0}\right)_{hetero} = -\alpha_{hetero}{}^{BR}(\alpha\beta)_{NP-NC}N_{NP}N_{NC} \quad (2)$$

These equations describe the initial rate of change in the number concentration of unaggregated ENPs ($dN_{NP}/dt|_{t\to 0}$) via homo- or heteroaggregation at early times (see Supplementary Information for details). In Equations 1 and 2, the terms α_{homo} and α_{hetero} are attachment efficiencies denoting the likelihood that two colliding particles will attach to form a larger aggregate.

The precise value of these parameters is unknown; however, the trends predicted according Equations 1 and 2 can be compared with the experimental results to identify the relative importance of each process (i.e. homo- and heteroaggregation) and provide insights into the relationship between α_{homo} and α_{hetero}. This is accomplished by recognizing that in the filtered WRW, the loss of ENPs via aggregation can be modelled according to Equation 1. Since both homo- and heteroaggregation can occur simultaneously within the raw WRW, the loss of ENPs

via aggregation in the raw WRW is more accurately modelled by the total initial aggregation rate (i.e., the summation of Equations 1 and 2). The ratio of the initial aggregation rates within these two experimental systems can then be compared according to Equation 3.

$$\frac{\left(\frac{dN_{NP}}{dt}|_{t\to 0}\right)_{homo}}{\left(\frac{dN_{NP}}{dt}|_{t\to 0}\right)_{homo}+\left(\frac{dN_{NP}}{dt}|_{t\to 0}\right)_{hetero}}=\frac{1}{1+\chi\left(\frac{BR_{(\alpha\beta)_{NC-NP}}N_{NC}}{BR_{(\alpha\beta)_{NP-NP}}N_{NP}}\right)} \quad (3)$$

with $=\frac{\alpha_{hetero}}{\alpha_{homo}}$, where values of $\chi < 1$ indicate $\alpha_{homo} > \alpha_{hetero}$ whereas $\chi > 1$ indicate $\alpha_{homo} < \alpha_{hetero}$.

Using the inputs discussed previously and the range $\chi = [10^{-3}\ 10^{3}]$, Equation 3 can be plotted as a function of d_{NC} to convey the importance of homoaggregation alone versus the combination of homo- and heteroaggregation. According to Equation 3, the removal of the model ENPs via heteroaggregation becomes increasing negligible relative to removal via homoaggregation as the ordinate approaches 1. Defining a criterion where the loss of ENPs via heteroaggregation is ≤ 10% of the loss via homoaggregation, it is possible to delineate relevant combinations of χ and d_{NC}.

As shown in Figure 3, there are two overall conditions that satisfy this criterion: (1) either $\chi \leq 1$ must be true (regardless of d_{NC}) or (2) if $\chi > 1$, then d_{NC} must be increasingly larger the greater χ becomes. For example, at $\chi = 10$ (i.e., $\alpha_{hetero} = 10x\ \alpha_{homo}$), for the loss of the model ENPs via heteroaggregation to be less than 10% of the loss via homoaggregation, $d_{NC} \geq 590$ nm. As noted previously, the similarity in η measured in the filtered and raw WRW reveals that in our experimental system heteroaggregation was negligible relative to homoaggregation. As the

majority of the NCs are expected to have $d_{NC} \ll 1$ µm, the second condition is unlikely to have been attained in our experimental system and therefore suggests that $\chi \leq 1$ was likely valid (i.e., $\alpha_{homo} \geq \alpha_{hetero}$).

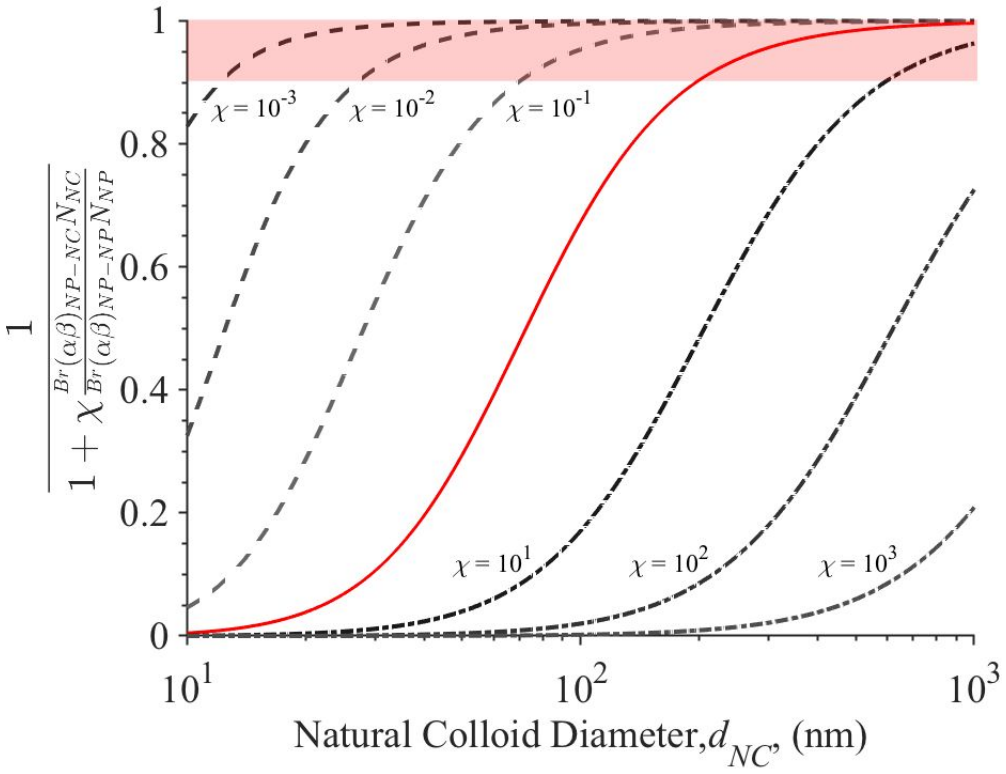

Figure 3. Ratio of initial aggregation rate ($dN_{NP}/dt|_{t\to 0}$) due to homoaggregation alone to combination of homo- and heteroaggregation as a function of d_{NC}, with $\chi = [10^{-3} - 10^{3}]$ where (dashed) $\chi < 1$, (red) $\chi = 1$, and (dash-dot) $\chi > 1$. Red box denotes region where $dN_{NP}/dt|_{t\to 0}$ from heteroaggregation is ≤ 10% of $dN_{NP}/dt|_{t\to 0}$ from homoaggregation.

Why homoaggregation was more favorable than heteroaggregation is unclear; however, this finding illustrates the importance of the processes accounted for by α that are currently not understood but nonetheless influence the outcome of particle-particle interactions. One of these processes is eco-corona formation via NOM adsorption. For cationic surface coatings, such

as the PEG-Amine and bPEI, the initial positive charge provided by the engineered surface coatings should promote heteroaggregation with the negatively-charged NCs as well as the adsorption of NOM.

The finding that heteroaggregation was negligible suggests that eco-corona formation occurred faster than heteroaggregation. It has been previously shown that the negative surface charge and steric interactions provided by adsorbed NOM can hinder heteroaggregation.[20,23,43] This phenomena could explain the results of the current work. For this to occur, the characteristic timescale for eco-corona formation must be less than that for heteroaggregation. Nason et al. (2012) reported that the adsorption of various model NOMs to the surface of Cit-AuNPs occurred relatively fast and was complete after only a few minutes. Using $dN_{NP}/dt|_{t\to 0}$ for heteroaggregation, the characteristic time for heteroaggregation ($t_{char,hetero}$) was calculated (see Supplementary Information for details). At d_{NC} = 500 nm (the mid-point of d_{NC} = 10^2 – 10^3 nm), $t_{char,hetero}$ was estimated between approximately 400 – 4.3 $x10^6$ s across the range of $10^0 > \alpha_{hetero} > 10^{-4}$ (Figure S6). While dependent on both the assumed value of d_{NC} and α_{hetero}, the estimates reveal that $t_{char,hetero}$ was on the order of 10^2 s or higher and, therefore, likely greater than the characteristic time for eco-corona formation reported by Nason et al. (2012).

In the current work, if the eco-corona formation outpaced ENP-NC heteroaggregation then the eco-corona formed via NOM adsorption would dictate the outcome of particle-particle interactions. Focusing on the raw WRW, this would suggest that at early times immediately after introducing the model ENPs there are, in essence, two types of particles in the system—ENPs with low fractional NOM surface coverage and NCs with the maximum fractional NOM surface coverage for the conditions of the WRW. The latter particle type is likely since the adsorption/desorption of NOM to the surface of the NCs is expected to be at equilibrium. It is hypothesized that homoaggregation between two ENPs partially-coated with NOM is more favorable than heteroaggregation between an ENP partially-coated with NOM and an NC fully-

coated with NOM. This hypothesis is supported by comparing $t_{char,homo}$ and $t_{char,hetero}$, wherein it was found that within the range of $10^2 < d_{NC} < 10^3$ nm, $t_{char,homo}$ was consistently less than $t_{char,hetero}$ whenever $\alpha_{homo} \geq \alpha_{hetero}$ (Figure S6). This phenomena may reflect the increasing importance of steric interactions that arise as the NOM surface coverage increases, especially under relatively low ionic strengths.[21,44]

In light of these aspects, it is hypothesized that the combined ratio of [NOM]:N_{NP}:N_{NC} dictates both particle stability and the mode of aggregation in natural aquatic mediums. For ENPs that readily adsorb NOM, variations in the [NOM]:[ENP] ratio (functionally equivalent to [NOM]:N_{NP}) have been shown to either stabilize the ENPs via overcoating by NOM or to promote their aggregation.[25] This phenomena is likely a function of the total surface area available for NOM adsorption, with changes in [NOM], NOM composition and N_{NP} (which is tied to d_{NP}) affecting the amount of NOM adsorbed to the surface of the ENPs. The impact of [NOM]:N_{NP} can be interpreted as altering α_{homo} and α_{hetero}, which the current work demonstrates can favor one aggregation process over the other. Likewise, the number concentration ratio of N_{NP}:N_{NC} will also dictate the dominant mode of aggregation. If homoaggregation and heteroaggregation are both favorable and $N_{NP} \ll N_{NC}$, then heteroaggregation will be more relevant whereas if $N_{NP} \approx N_{NC}$ or $N_{NP} \gg N_{NC}$, then homoaggregation will be increasingly important.

The conceptual relationship between [NOM]:N_{NP}:N_{NC} is shown in Figures 4 and 5. When ENPs enter an aquatic system containing NOM and NCs, there are several possible outcomes (Figure 4). In cases where there are favorable interactions between NOM and the ENPs (e.g., positively-charged ENPs), a competition is set-up between (1) eco-corona formation on the ENPs via NOM adsorption and (2) aggregation (homo- or heteroaggregation). Whether homo- or heteroaggregation will be dominant is dependent on N_{NP}:N_{NC} and their associated attachment efficiencies (α). When NOM concentrations are high relative to the available ENP and NC concentrations/surface areas, the system is driven towards fully coated ENPs and α_{homo} and

α_{hetero} tend toward zero (Figure 5). Furthermore, if NOM interactions are relatively fast, as was reported in Nason et al. (2012), it is these initial interactions with NOM that ultimately dictate α.

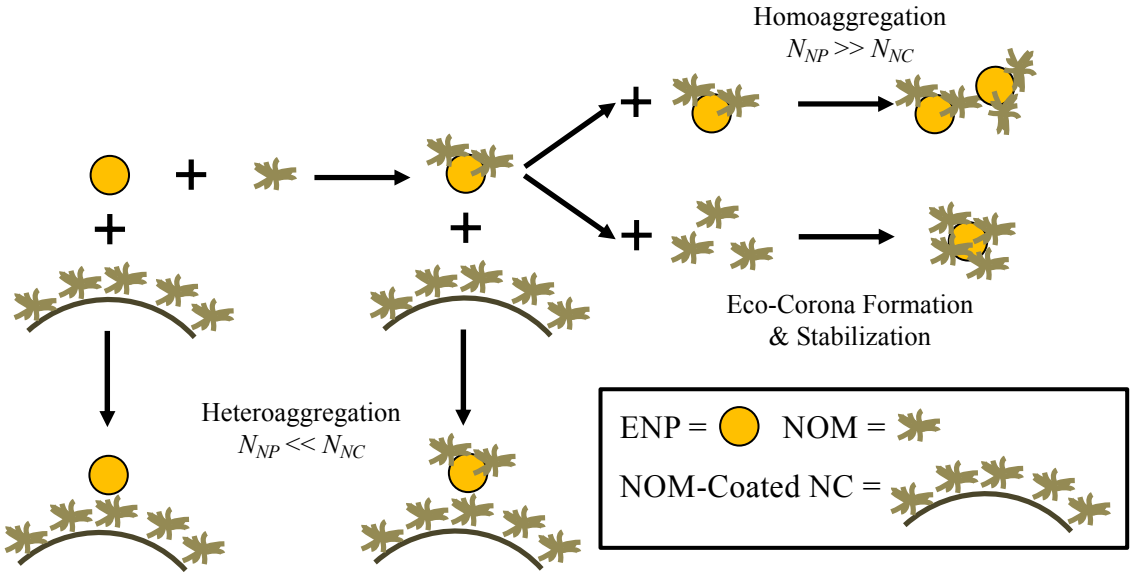

Figure 4. Conceptual reactions taking place upon addition of an ENP to an aquatic system containing NOM and NCs. In this illustrative example, NOM-NP interactions are assumed to be favorable, while ENP-ENP interactions are unfavorable.

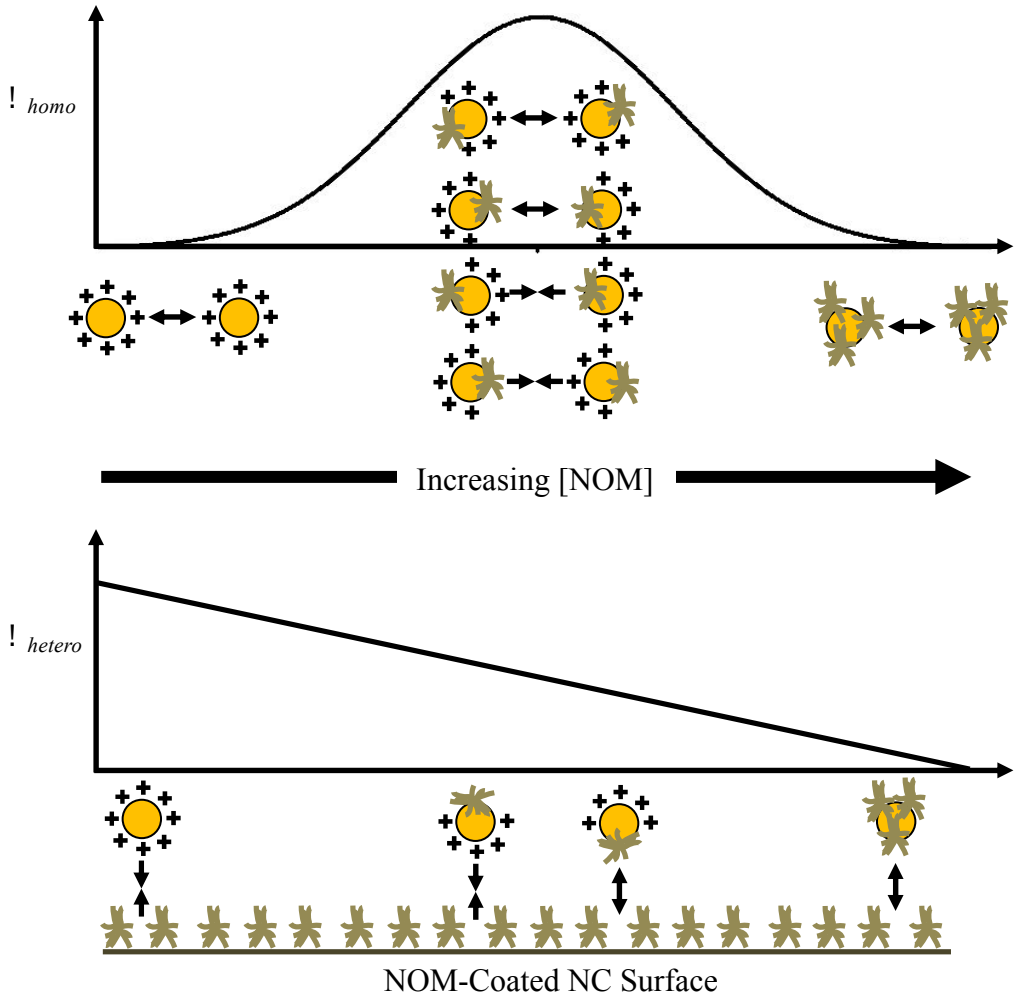

Figure 5. Conceptual variation of α_{homo} and α_{hetero} for a positively-charged ENP as a function of [NOM] at fixed N_{NP} and N_{NC}.

In the current work we found that the [NOM]:N_{NP}:N_{NC} employed resulted in a system that favored homoaggregation of model ENPs that readily adsorbed NOM while the model ENPs that did not form an eco-corona or for which interactions with NOM did not promote aggregation were stable. This finding highlights the importance of considering all three factors during experimental design. As all three components are linked, altering one factor can affect both ENP colloidal stability and the dominant mode of aggregation. Clearly, there are challenges that limit

the extent to which [NOM]:N_{NP}:N_{NC} can match realistic environmental conditions. Namely, N_{NP} is often much higher than is expected in the environment. While this is currently difficult to avoid due to analytical limitations, the findings from the current work illustrate the importance of considering this factor, along with [NOM] and N_{NC}, in interpreting experimental results.

Overall, the batch experiments using the raw WRW reveal that variations in the properties of the engineered surface coatings continue to influence particle-particle interactions in a complex aquatic medium. The PEG- and PEG-COOH-AuNPs were stable in both the filtered and raw WRW while the PEG-Amine-, bPEI-, and Cit-AuNPs were unstable and aggregated. Comparing the results of the filtered and raw WRW batch experiments helps highlight the importance of two competing processes—eco-corona formation and aggregation. The results using the filtered WRW show that the former process is dictated by an ENP's engineered surface coatings. Once destabilized, the dominant mode of aggregation affecting the ENPs is dependent on the relative amounts of ENPs and NCs, as well as the rate and extent of eco-corona formation. Taken as a whole, it is hypothesized that a combination of factors, expressed through the combined ratio of [NOM]:N_{NP}:N_{NC}, will dictate particle stability and the dominant aggregation process affecting the fate and transport of the ENPs.

Surface Affinity Functional Assay

To aid the modelling of ENP aggregation in complex aquatic mediums, we attempted to translate the results from the batch experiments into estimates of α_{homo} and α_{hetero}. To achieve this, the surface affinity functional assay developed by Wiesner and colleagues was evaluated.[26–30] According to Hendren et al. (2015), functional assays are defined as "procedures for quantifying parameters that describe a specific process (or function) occurring within a given (often complex) system". Functional assays are intended to serve as a bridge between simplified model systems and complex environmental systems. The surface affinity functional assay relies

on measuring the number concentration of ENPs remaining in suspesion ($N_{NP,i}$) as a function of time.[26,28] The overall slope determined via linear regression can then be used to extract the value of α_{hetero} (Equation 4).

$$\ln\left(\frac{N_{NP,0}}{N_{NP,i}}\right) = -\alpha_{hetero}{}^{TOT}(\alpha\beta)_{NP-NC}N_{NC}t \quad (4)$$

In Equation 4, $N_{NP,0}$ is the initial ENP number concentration, while the other terms have been previously defined.

The process of estimating α_{hetero} using the surface affinity functional assay is accomplished through certain assumptions and specific components of the experimental design. First, the method assumes that the loss of ENPs via homoaggregation is negligible. Within certain mediums this assumption is reasonable, such as investigating ENP aggregation within activated sludge where N_{NP} is known to be much less than N_{NC}.[46,47] Alternatively, this requirement can be achieved by using background colloid concentrations much higher than those expected in the environment or by selecting ENPs that are stable with respect to homoaggregation.[27–30] Using this assumption, α_{hetero} can then be extracted from the slope of the linear regression by two approaches—dividing by estimated values of ${}^{TOT}(\alpha\beta)_{NP\text{-}NC}$ N_{NC} or normalizing the slope by that measured when aggregation is favorable (i.e., $\alpha_{hetero} \rightarrow 1$). The former can be realized if the properties and number concentration of the colloids are known (e.g., monodisperse and homogeneous model colloids) or are accurately measured. Otherwise, in cases where either ${}^{TOT}(\alpha\beta)_{NP\text{-}NC}$ is difficult to calculate and/or N_{NC} is unknown, the latter approach can be used to derive 'relative' surface affinities.

In designing the current research, we chose to work with the experimental conditions presented by an actual environmental medium. While higher than is expected in the environment, N_{NP} in the current work was significantly lower than in previous tests using the surface affinity functional assay.[26–29] Likewise, the NC mass concentration (3.9 ± 0.4 mg/L) of the WRW was orders of magnitude lower than previous research applying the surface affinity functional assay. Under these conditions, we found that removal via homoaggregation alone was comparable to the combined effect of homo- and heteroaggregation (Figure 1a). This finding indicates that the main assumption underlying the surface affinity functional assay was not valid for our experimental system. Specifically, the method requires that the loss of AuNPs is attributable to heteroaggregation alone. Ignoring this finding and deriving values of α_{hetero} according to the approach would not have served the purpose of refining ENP environmental fate modelling and thus was not attempted.

Even if the assumption that homoaggregation was negligible was valid, incorporating an actual environmental medium into the experimental design generated significant uncertainties when estimating the value of α_{hetero}. First, both N_{NC} and d_{NC} of the native NCs must be measured. Currently, there is no analytical technique that can provide a particle size distribution (PSD) spanning the low-nanometer-to-high-micrometer size range. Overlaying the PSDs from multiple techniques, such as combining the PSD measured via single-particle inductively-coupled plasma mass spectrometry (sp-ICP-MS) or nanoparticle tracking analysis (NTA) with the PSD measured via Coulter Counter presents numerous of challenges, the least of which is identifying and quantifying NCs that are an assemblage of particles from myriad biogenic and geogenic origins. Second, as the derivation of α_{hetero} is dependent upon the estimation of ${}^{TOT}(\alpha\beta)_{NP\text{-}NC}$ and N_{NC}, errors in either of these parameters directly transfer to the estimated value of α_{hetero}. This concern was addressed in Geitner et al. (2017) by calculating the 'relative surface affinity' and eliminating the need to calculate ${}^{TOT}(\alpha\beta)_{NP\text{-}NC}$ and N_{NC}. Unfortunately, such a condition may not be realized or even feasible when working with actual environmental systems. Complicating matters is the dependence of ${}^{TOT}(\alpha\beta)_{NP\text{-}NC}$ on an accurate estimation of d_{NC}, which is linked to the

issues noted previously. These challenges help to highlight some of the current limitations associated with the surface affinity functional assay.

The surface affinity functional assay does provide a method to calculate α_{hetero} and has been useful under conditions where the above issues are negligible or can be mitigated. The results from the current study simply suggest that this assay may not be readily applicable to all environmental systems of interest. More importantly, the current work highlights the care that must be taken during experimental design to consider how relative changes in [NOM], N_{NP}, and N_{NC} can significantly alter the experimental outcomes. Attempts to simplify the assay or employing conditions that are amenable to the experimental objectives may have unintended (and potentially unknown) consequences and prevent important insights. Referring back to Figures 4 and 5, it is clear that if N_{NP} and N_{NC} are manipulated independently from [NOM], the system may be biased towards a condition not representative of the actual system under study. For example, if N_{NP} were increased relative to [NOM] (equivalent to reducing [NOM] in Figure 5) the result would be increases in both α_{homo} and α_{hetero}. To our knowledge, this potential unintended consequence of the design of the surface affinity functional assay has not yet been explored and deserves additional attention. For example, strategies are needed to guide the appropriate selection of relative [NOM] in instances where it is desirable to employ elevated N_{NP} and N_{NC}.

Under the conditions employed in the current work, it was deemed inappropriate to estimate α_{hetero}. While this prevented us from achieving our second objective, the findings nonetheless serve to demonstrate the relevance of engineered surface coatings through their influence on ENP aggregation within an actual aquatic medium. Working within a complex natural medium presents various complications. Yet, it remains important to move investigations of relevant processes and factors affecting ENP environmental fate from simplistic model systems to more

complex environmental systems to fully capture the interrelated and dynamic processes inherent in the latter.

Implications on ENP Environmental Fate

In spite of the complications in applying the surface affinity functional assay, this work demonstrated the role engineered surface coatings play in influencing ENP aggregation behavior. More specifically, they show that certain engineered surface coatings have the ability to stabilize ENPs against both homo- and heteroaggregation in a complex aquatic medium while other surface coatings can promote aggregation through eco-corona formation. Furthermore, comparing trends between the filtered and raw WRW provides further evidence that the interaction between natural macromolecules and ENPs can strongly influence ENP colloidal stability.

In modelling the environmental fate of ENPs, Sani-Kast et al. (2015) found that the properties of the local environment near the point where ENPs are released (e.g., waters receiving the effluent from a wastewater treatment plant) is a strong predictor of environmental fate. If conditions favor aggregation, then the ENPs are more likely to end up in the local sediments where their environmental fate is linked to sediment transport processes.[49] Conversely, if the ENPs are stable near the point of discharge then they can remain mobile and be transported further downstream. With this in mind, the results from the batch experiments suggest that the PEG- and PEG-COOH-AuNPs are likely to remain mobile upon their discharge to a natural freshwater environment, whereas the PEG-Amine-, bPEI-, and Cit-AuNPs would aggregate and become associated with the localized sediments.

CONCLUSIONS

The primary aim of this research was to determine if an ENP's engineered surface coating can influence their colloidal stability in a complex aquatic medium. Of the five model ENPs tested, two were colloidally stable (PEG- and PEG-COOH-AuNPs) while the other three were destabilized and removed to varying degrees via aggregation (PEG-Amine-, bPEI-, and Cit-AuNPs). By employing a combination of techniques, we found that various properties of the engineered surface coatings can influence ENP colloidal stability. These include their surface charge, stabilization mechanism, and core-coating binding mechanism. The surface charge of the engineered surface coating was shown to influence eco-corona formation. In cases where NOM adsorption is not favorable and the engineered surface coating is strongly bound to the ENP core (e.g., neutral- or negatively-charged and covalently-bound), the stabilization mechanism can dictate ENP colloidal stability. If the engineered surface coating is weakly bound (e.g., electrostatics), then surface coating displacement via NOM adsorption can occur. Finally, when NOM adsorption is favorable (or the surface coating is displaceable via NOM), the eco-corona formed on the ENP can result in their aggregation through a variety of mechanisms, including interparticle bridging, divalent cation bridging, and localized charge neutralization. However, it should be noted that whether eco-corona formation destabilizes or stabilizes the ENPs is also linked to the ratio of [NOM]:N_{NP} as well as the aquatic chemistry (i.e., ionic strength and composition).

The second intent of this work was to refine the modelling of ENP aggregation by applying the surface affinity functional assay to derive estimates of α_{hetero}. However, a number of limitations were identified that hindered this goal. Homoaggregation was not negligible at the experimental conditions of the current work, a key assumption of the assay. Furthermore, the method relies upon the accurate measurement of N_{NC} and d_{NC}, which are difficult to estimate in a complex environmental medium. Although these limitations have been circumvented through the use of elevated concentrations of model NCs in natural systems[27–30], we suggest that the use of elevated N_{NP} and N_{NC} must be carefully considered relative to the role of NOM in controlling NC and ENP surface properties and attachment efficiencies. We hypothesize that the relative

concentrations of [NOM]:N_{NP}:N_{NC} will dictate both colloidal stability and the dominant mode of aggregation. In general, it is recommended that the relative ratios of these three components be considered during experimental design. Ideally, these factors should mimic the expected environmental conditions for the system under investigation. When that is not feasible, consideration should be given to adjusting the experimental design in a way that allows [NOM]:N_{NP}:N_{NC} to reasonably match realistic environmental conditions. Through additional work it is expected that these challenges can be minimized so that the functional assay can be applied to a broader range of environmental systems.

While the research presented here utilized an actual environmental medium to investigate ENP aggregation, there is additional progress to be made in the push towards 'true' environmental relevancy. In particular, it is unlikely that 'pristine' ENPs, as used in this research, will be directly released to the environment. Instead, recent research has emphasized the importance of considering an ENP's life-cycle to fully capture the various transformations (termed 'aging') that might alter an ENP's properties during its production, use, and eventual release.[50–52] Recent investigations also suggest that seasonal variations in the chemistry of the aquatic medium may have surface coating-specific effects.[18] Thus, future research will need to shift towards utilizing aged ENPs and investigating the role of changing aquatic chemistry to fully define the dominant factors controlling ENP environmental fate.

ASSOCIATED CONTENT

SUPPLEMENTARY INFORMATION

Electronic Supplementary Information (ESI) available, including characterization of the model ENPs and WRW, TR-DLS plots for each AuNP type in the filtered WRW, details regarding the modelled collision frequencies and initial aggregation rates, and ancillary tests performed to support the experimental design.

AUTHOR INFORMATION

Corresponding Author

* Email: Jeff.Nason@oregonstate.edu Phone:(541) 737-9911 Fax (541) 737-4600.

CONFLICTS OF INTEREST

There are no conflicts of interest to declare.

ACKNOWLEDGEMENTS

This research was supported by the National Science Foundation (NSF) Graduate Research Fellowship Program under Grant No. DGE-1314109 and NSF Grant No. 1255020. Any opinions, findings, and conclusions or recommendations expressed in this material are those of the author(s) and do not necessarily reflect the views of the NSF. Special thanks to A. Ungerer (W.M. Keck Collaboratory) for assistance with the ICP-OES measurements; K. Motter (IWW

Collaboratory) for assistance with TOC/DOC measurements; A. Deline, J. Fiest, and A. Bernstein Livne for assistance during the batch experiments; and J. Laurance for assistance with the TR-DLS and EPM measurements.

REFERENCES

1 S. Wagner, A. Gondikas, E. Neubauer, T. Hofmann and F. von der Kammer, Spot the Difference: Engineered and Natural Nanoparticles in the Environment-Release, Behavior, and Fate, *Angew. Chemie Int. Ed.*, 2014, **53**, 12399–12419.

2 S. J. Klaine, P. J. J. Alvarez, G. E. Batley, T. F. Fernandes, R. D. Handy, D. Y. Lyon, S. Mahendra, M. J. McLaughlin and J. R. Lead, Nanomaterials in the Environment: Behavior, Fate, Bioavailability, and Effects, *Environ. Toxicol. Chem.*, 2008, **27**, 1825.

3 J. Meesters, A. A. Koelmans, J. T. K. Quik, A. J. Hendriks and D. Van De Meent, Multimedia modeling of engineered nanoparticles with simpleBox4nano: Model definition and evaluation, *Environ. Sci. Technol.*, 2014, **48**, 5726–5736.

4 H. H. Liu and Y. Cohen, Multimedia environmental distribution of engineered nanomaterials, *Environ. Sci. Technol.*, 2014, **48**, 3281–3292.

5 K. L. Garner, S. Suh and A. A. Keller, Assessing the Risk of Engineered Nanomaterials in the Environment: Development and Application of the nanoFate Model, *Environ. Sci. Technol.*, 2017, **51**, 5541–5551.

6 A. Praetorius, N. Tufenkji, K.-U. Goss, M. Scheringer, F. von der Kammer and M. Elimelech, The road to nowhere: equilibrium partition coefficients for nanoparticles, *Environ. Sci. Nano*, 2014, **1**, 317.

7 G. Cornelis, Fate descriptors for engineered nanoparticles: the good, the bad, and the ugly, *Environ. Sci. Nano*, 2015, **2**, 19–26.

8 A. L. Dale, G. V. Lowry and E. A. Casman, Much ado about α: reframing the debate over appropriate fate descriptors in nanoparticle environmental risk modeling, *Environ. Sci. Nano*, 2015, **2**, 27–32.

9 F. Gottschalk, T. Y. Sun and B. Nowack, Environmental concentrations of engineered nanomaterials: Review of modeling and analytical studies, *Environ. Pollut.*, 2013, **181**, 287–300.

10 M. Baalousha, G. Cornelis, T. A. J. Kuhlbusch, I. Lynch, C. Nickel, W. J. G. M. Peijnenburg and N. W. van den Brink, Modeling nanomaterial fate and uptake in the environment: current knowledge and future trends, *Environ. Sci. Nano*, 2016, **3**, 323–345.

11 A. L. Dale, E. A. Casman, G. V. Lowry, J. R. Lead, E. Viparelli and M. Baalousha, Modeling Nanomaterial Environmental Fate in Aquatic Systems, *Environ. Sci. Technol.*, 2015, **49**, 2587–2593.

12 A. Praetorius, R. Arvidsson, S. Molander and M. Scheringer, Facing complexity through informed simplifications: a research agenda for aquatic exposure assessment of nanoparticles, *Environ. Sci. Process. Impacts*, 2013, **15**, 161–168.

13 G. Raza, M. Amjad, I. Kaur, M. Baalousha, J. R. Lead and D. Wen, Stability and Aggregation Kinetics of Titania Nanomaterials under Environmentally Realistic Conditions, *Environ. Sci. Technol.*, 2016, **50**, 12525–12525.

14 J. A. Gallego-Urrea, J. Hammes, G. Cornelis and M. Hassellöv, Coagulation and sedimentation of gold nanoparticles and illite in model natural waters: Influence of initial particle concentration, *NanoImpact*, 2016, **3**–**4**, 67–74.

15 A. Philippe and G. E. Schaumann, Interactions of dissolved organic matter with natural and engineered inorganic colloids: A review, *Environ. Sci. Technol.*, 2014, **48**, 8946–8962.

16 S. M. Louie, E. R. Spielman-Sun, M. J. Small, R. D. Tilton and G. V. Lowry, Correlation of the Physicochemical Properties of Natural Organic Matter Samples from Different Sources to Their Effects on Gold Nanoparticle Aggregation in Monovalent Electrolyte, *Environ. Sci. Technol.*, 2015, **49**, 2188–2198.

17 F. Loosli and S. Stoll, Effect of surfactants, pH and water hardness on the surface properties and agglomeration behavior of engineered TiO_2 nanoparticles, *Environ. Sci. Nano*, 2016, **4**, 203–211.

18 L.-J. A. Ellis, M. Baalousha, E. Valsami-Jones and J. R. Lead, Seasonal variability of natural water chemistry affects the fate and behaviour of silver nanoparticles, *Chemosphere*, 2018, **191**, 616–625.

19 A. Praetorius, J. Labille, M. Scheringer, A. Thill, K. Hungerbühler and J. Bottero, Heteroaggregation of Titanium Dioxide Nanoparticles with Model Natural Colloids under Environmentally Relevant Conditions, *Environ. Sci. Technol.*, 2014, **48**, 10690–10698.

20 B. M. Smith, D. J. Pike, M. O. Kelly and J. A. Nason, Quantification of Heteroaggregation between Citrate-Stabilized Gold Nanoparticles and Hematite Colloids, *Environ. Sci. Technol.*, 2015, **49**, 12789–12797.

21 J. A. Nason, S. A. McDowell and T. W. Callahan, Effects of natural organic matter type and concentration on the aggregation of citrate-stabilized gold nanoparticles, *J. Environ. Monit.*, 2012, **14**, 1885.

22 M. Baalousha, Effect of nanomaterial and media physicochemical properties on nanomaterial aggregation kinetics, *NanoImpact*, 2017, **6**, 55–68.

23 S. M. Louie, R. D. Tilton and G. V. Lowry, Critical review: impacts of macromolecular

coatings on critical physicochemical processes controlling environmental fate of nanomaterials, *Environ. Sci. Nano*, 2016, **3**, 283–310.

24 D. P. Stankus, S. E. Lohse, J. E. Hutchison and J. A. Nason, Interactions between Natural Organic Matter and Gold Nanoparticles Stabilized with Different Organic Capping Agents, *Environ. Sci. Technol.*, 2011, **45**, 3238–3244.

25 M. C. Surette and J. A. Nason, Effects of surface coating character and interactions with natural organic matter on the colloidal stability of gold nanoparticles, *Environ. Sci. Nano*, 2016, **3**, 1144–1152.

26 L. E. Barton, M. Therezien, M. Auffan, J.-Y. Bottero and M. R. Wiesner, Theory and Methodology for Determining Nanoparticle Affinity for Heteroaggregation in Environmental Matrices Using Batch Measurements, *Environ. Eng. Sci.*, 2014, **31**, 421–427.

27 N. K. Geitner, S. M. Marinakos, C. Guo, N. O'Brien and M. R. Wiesner, Nanoparticle Surface Affinity as a Predictor of Trophic Transfer, *Environ. Sci. Technol.*, 2016, **50**, 6663–6669.

28 N. K. Geitner, N. J. O'Brien, A. A. Turner, E. J. Cummins and M. R. Wiesner, Measuring Nanoparticle Attachment Efficiency in Complex Systems, *Environ. Sci. Technol.*, 2017, **51**, 13288–13294.

29 B. P. Espinasse, N. K. Geitner, A. Schierz, M. Therezien, C. J. Richardson, G. V. Lowry, L. Ferguson and M. R. Wiesner, Comparative Persistence of Engineered Nanoparticles in a Complex Aquatic Ecosystem, *Environ. Sci. Technol.*, 2018, **52**, 4072–4078.

30 N. K. Geitner, J. L. Cooper, A. Avellan, B. T. Castellon, B. G. Perrotta, N. Bossa, M. Simonin, S. M. Anderson, S. Inoue, M. F. Hochella, C. J. Richardson, E. S. Bernhardt, G. V. Lowry, P. L. Ferguson, C. W. Matson, R. S. King, J. M. Unrine, M. R. Wiesner and H. Hsu-Kim, Size-Based Differential Transport, Uptake, and Mass Distribution of Ceria (CeO2) Nanoparticles in Wetland Mesocosms, *Environ. Sci. Technol.*, 2018, **52**, 9768–9776.

31 T. Karanfil, I. Erdogan and M. A. Schlautman, Selecting filter membranes DOC and SUVA254, *J. Am. Water Work. Assoc.*, 2003, **95**, 86–100.

32 M. S. Croughan, J.-F. Hamel and D. I. C. Wang, Hydrodynamic effects on animal cells grown in microcarrier cultures, *Biotechnol. Bioeng.*, 1987, **29**, 130–141.

33 K. L. Chen, B. A. Smith, W. P. Ball and D. H. Fairbrother, Assessing the colloidal properties of engineered nanoparticles in water: case studies from fullerene C 60 nanoparticles and carbon nanotubes, *Environ. Chem.*, 2010, **7**, 10.

34 S. M. Louie, R. D. Tilton and G. V. Lowry, Effects of molecular weight distribution and chemical properties of natural organic matter on gold nanoparticle aggregation., *Environ. Sci. Technol.*, 2013, **47**, 4245–54.

35 S. A. McDowell. The Effect of Engineered Coatings and Natural Organic Matter on Nanoparticle Aggregation (M.S. Thesis), 2012, Oregon State University, Corvallis, OR.

36 G. S. Perera, S. A. Athukorale, F. Perez, C. U. Pittman and D. Zhang, Facile displacement of citrate residues from gold nanoparticle surfaces, *J. Colloid Interface Sci.*, 2018, **511**, 335–343.

37 J. R. Lead and K. J. Wilkinson, Aquatic Colloids and Nanoparticles: Current Knowledge and Future Trends, *Environ. Chem.*, 2006, **3**, 159.

38 W. J. G. M. Peijnenburg, M. Baalousha, J. Chen, Q. Chaudry, F. Von der kammer, T. A. J. Kuhlbusch, J. R. Lead, C. Nickel, J. T. K. Quik, M. Renker, Z. Wang and A. a. Koelmans, A Review of the Properties and Processes Determining the Fate of Engineered Nanomaterials in the Aquatic Environment, *Crit. Rev. Environ. Sci. Technol.*, 2015, **45**, 2084–2134.

39 M. Baalousha, F. Von der Kammer, M. Motelica-Heino, M. Baborowski, C. Hofmeister and P. Le Coustumer, Size-Based Speciation of Natural Colloidal Particles by Flow Field Flow Fractionation, Inductively Coupled Plasma-Mass Spectroscopy, and Transmission Electron Microscopy/X-ray Energy Dispersive Spectroscopy: Colloids−Trace Element Interaction, *Environ. Sci. Technol.*, 2006, **40**, 2156–2162.

40 M. Baalousha, F. von der Kammer, M. Motelica-Heino, H. S. Hilal and P. Le Coustumer, Size fractionation and characterization of natural colloids by flow-field flow fractionation coupled to multi-angle laser light scattering, *J. Chromatogr. A*, 2006, **1104**, 272–281.

41 H. P. Jarvie and S. M. King, Small-Angle Neutron Scattering Study of Natural Aquatic Nanocolloids, *Environ. Sci. Technol.*, 2007, **41**, 2868–2873.

42 M. Han and D. F. Lawler, The (Relative) Insignificance of G in Flocculation, *J. Am. Water Work. Assoc.*, 1992, **84**, 79–91.

43 A. A. Keller, H. Wang, D. Zhou, H. S. Lenihan, G. Cherr, B. J. Cardinale, R. Miller and J. I. Zhaoxia, Stability and aggregation of metal oxide nanoparticles in natural aqueous matrices, *Environ. Sci. Technol.*, 2010, **44**, 1962–1967.

44 L. M. Mosley, K. A. Hunter and W. A. Ducker, Forces between Colloid Particles in Natural Waters, *Environ. Sci. Technol.*, 2003, **37**, 3303–3308.

45 C. O. Hendren, G. V. Lowry, J. M. Unrine and M. R. Wiesner, A functional assay-based

strategy for nanomaterial risk forecasting, *Sci. Total Environ.*, 2015, **536**, 1029–1037.

46 R. Kägi, A. Voegelin, B. Sinnet, S. Zuleeg, H. Hagendorfer, M. Burkhardt and H. Siegrist, Behavior of Metallic Silver Nanoparticles in a Pilot Wastewater Treatment Plant, *Environ. Sci. Technol.*, 2011, **45**, 3902–3908.

47 R. Kägi, A. Voegelin, C. Ort, B. Sinnet, B. Thalmann, J. Krismer, H. Hagendorfer, M. Elumelu and E. Mueller, Fate and transformation of silver nanoparticles in urban wastewater systems, *Water Res.*, 2013, **47**, 3866–3877.

48 N. Sani-Kast, M. Scheringer, D. Slomberg, J. Labille, A. Praetorius, P. Ollivier and K. Hungerbühler, Addressing the complexity of water chemistry in environmental fate modeling for engineered nanoparticles., *Sci. Total Environ.*, 2015, **535**, 150–159.

49 A. L. Dale, G. V. Lowry and E. A. Casman, Stream Dynamics and Chemical Transformations Control the Environmental Fate of Silver and Zinc Oxide Nanoparticles in a Watershed-Scale Model, *Environ. Sci. Technol.*, 2015, **49**, 7285–7293.

50 D. M. Mitrano, S. Motellier, S. Clavaguera and B. Nowack, Review of nanomaterial aging and transformations through the life cycle of nano-enhanced products, *Environ. Int.*, 2015, **77**, 132–147.

51 D. M. Mitrano and B. Nowack, The need for a life-cycle based aging paradigm for nanomaterials: importance of real-world test systems to identify realistic particle transformations, *Nanotechnology*, 2017, **28**, 072001.

52 B. Nowack and D. M. Mitrano, Procedures for the production and use of synthetically aged and product released nanomaterials for further environmental and ecotoxicity testing, *NanoImpact*, 2018, **10**, 70–80.

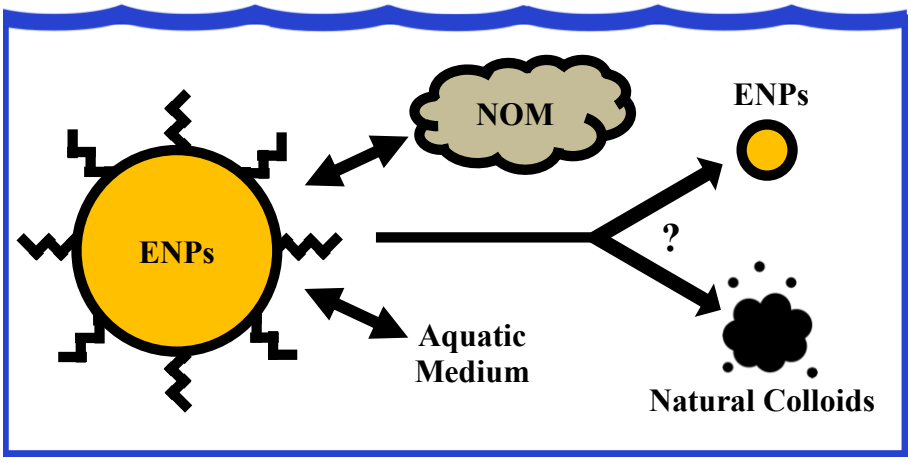

Surface coatings applied to ENPs alter eco-corona formation in complex aquatic matrices, affecting homo- and heteroaggregation processes and environmental fate.